

Close relationship between superconductivity and the bosonic mode in $\text{Ba}_{0.6}\text{K}_{0.4}\text{Fe}_2\text{As}_2$ and $\text{Na}(\text{Fe}_{0.975}\text{Co}_{0.025})\text{As}$

Zhenyu Wang^{1,2†}, Huan Yang^{1†}, Delong Fang¹, Bing Shen², Qiang-Hua Wang¹, Lei Shan², Chenglin Zhang³, Pengcheng Dai^{2,3} and Hai-Hu Wen^{1*}

Since the discovery in 2008 of high-temperature superconductivity in the iron pnictides and chalcogenides, a central issue has been the microscopic origin of the superconducting pairing. In particular, it remains unclear whether there is a bosonic mode from the tunnelling spectrum, which has a close and universal relationship with superconductivity as well as with the observed spin excitation. Here, on the basis of measurements of scanning tunnelling spectroscopy, we show clear evidence of a bosonic mode with energy identical to that of the neutron spin resonance in two completely different systems, $\text{Ba}_{0.6}\text{K}_{0.4}\text{Fe}_2\text{As}_2$ and $\text{Na}(\text{Fe}_{0.975}\text{Co}_{0.025})\text{As}$, with different superconducting transition temperatures. In both samples, the superconducting coherence peaks and the mode feature vanish simultaneously inside the vortex core or above the transition temperature T_c , indicating a close relationship between superconductivity and the bosonic mode. Our data also demonstrate a universal ratio between the mode energy and superconducting transition temperature, that is $\Omega/k_B T_c \approx 4.3$, which underlines the unconventional nature of superconductivity in the iron pnictide superconductors.

According to the Bardeen–Cooper–Schrieffer theory, the superconducting state is achieved by the quantum condensation of paired electrons, and the electron pairing is provided by the electron–phonon interaction. The compelling evidence for this model was the tunnelling spectrum dI/dV versus V , on which some fine structures, due to the electron–phonon coupling, appear at voltages of $\Delta + \Omega$ (or at $-\Delta - \Omega$), where Δ is the superconducting gap and Ω is the energy of a typical phonon mode^{1–4}. Hence, clear dips (or peaks) should be observed in the second derivative of the tunnelling curve, that is, d^2I/dV^2 versus V at energies of $\Delta + \Omega$ (or at $-\Delta - \Omega$). This is because the energy-dependent gap function $\Delta(\varepsilon)$, when taking the electron–phonon coupling into account, shows anomalies at $\Delta + \Omega$ (or at $-\Delta - \Omega$) and thus influences the quasi-particle density of states (DOS), which is proportional to dI/dV (refs 1–4). Inspired by this interesting scenario, it was found that a similar anomaly appeared outside the gap in the hole-doped cuprate $\text{Bi}_2\text{Sr}_2\text{CaCu}_2\text{O}_{8+\delta}$ measured by scanning tunnelling microscopy⁵ (STM), although it was argued that this peak–dip–hump feature might not be relevant for superconductivity, but resulted from inelastic tunnelling through the insulating oxide layers⁶ or simply from some Einstein mode of phonons⁷. For the electron-doped high- T_c cuprate superconductor $\text{Pr}_{0.88}\text{LaCe}_{0.12}\text{CuO}_4$, STM measurements have revealed a bosonic excitation at an energy of 10.5 meV, which is consistent with the neutron spin resonance energy, thus indicating spin-fluctuation-mediated superconductivity in this material^{8–10}. In the iron pnictide/chalcogenide superconductors, one of the proposed pictures for the pairing is through exchanging the antiferromagnetic spin fluctuations with the two electrons on the electron (hole) pockets,

and they are scattered to the hole (electron) pockets leading to a pairing order parameter with opposite signs on the electron and hole pockets; this is termed as the S_{\pm} pairing model^{11,12}. Inelastic neutron scattering data have given some preliminary evidence for this pairing gap; namely, a resonance peak appears at the momentum $Q = (\pi, 0)$ (in the unfolded Brillouin zone)¹³. In addition, some evidence to support this model is inferred from the quasi-particle interference pattern based on the spatial mapping of the local DOS (LDOS) in the STM measurements in Fe(Se,Te) (ref. 14). Therefore, it is interesting to determine whether the tunnelling spectrum dI/dV versus V exhibits some anomalies related to the neutron resonance or the unique S_{\pm} pairing. Recently, a dip–hump feature in the scanning tunnelling spectroscopy (STS) spectrum of an optimally hole-doped BaFe_2As_2 has been observed, and the mode energy seems to be close to the neutron spin resonance energy¹⁵. However, it is still possible that the mode is induced by the interaction between the electrons and a phonon mode. Here we present evidence for this bosonic mode in two totally different systems with different superconducting transition temperatures (T_c). These data suggest a close relationship between superconductivity and the bosonic mode associated with spin excitations instead of phonons.

Figure 1a shows a topographic image of the $\text{Ba}_{0.6}\text{K}_{0.4}\text{Fe}_2\text{As}_2$ sample measured by our STM with a tunnelling current $I_t = 200$ pA and a bias voltage $V = 40$ mV. The atomically resolved structure is clearly seen. The inset to Fig. 1a shows a closer view of the topography; the atomic structure turns out to be a square lattice with a constant of 5.4 Å with a mixture of white and dark spots on the image. By counting the numbers of the white and dark spots,

¹Center for Superconducting Physics and Materials, National Laboratory of Solid State Microstructures and Department of Physics, Nanjing University, Nanjing 210093, China, ²National Laboratory for Superconductivity, Institute of Physics and National Laboratory for Condensed Matter Physics, Chinese Academy of Sciences, Beijing 100190, China, ³Department of Physics and Astronomy, The University of Tennessee, Knoxville, Tennessee 37996-1200, USA. [†]These authors contributed equally to this work. *e-mail: hhwen@nju.edu.cn.

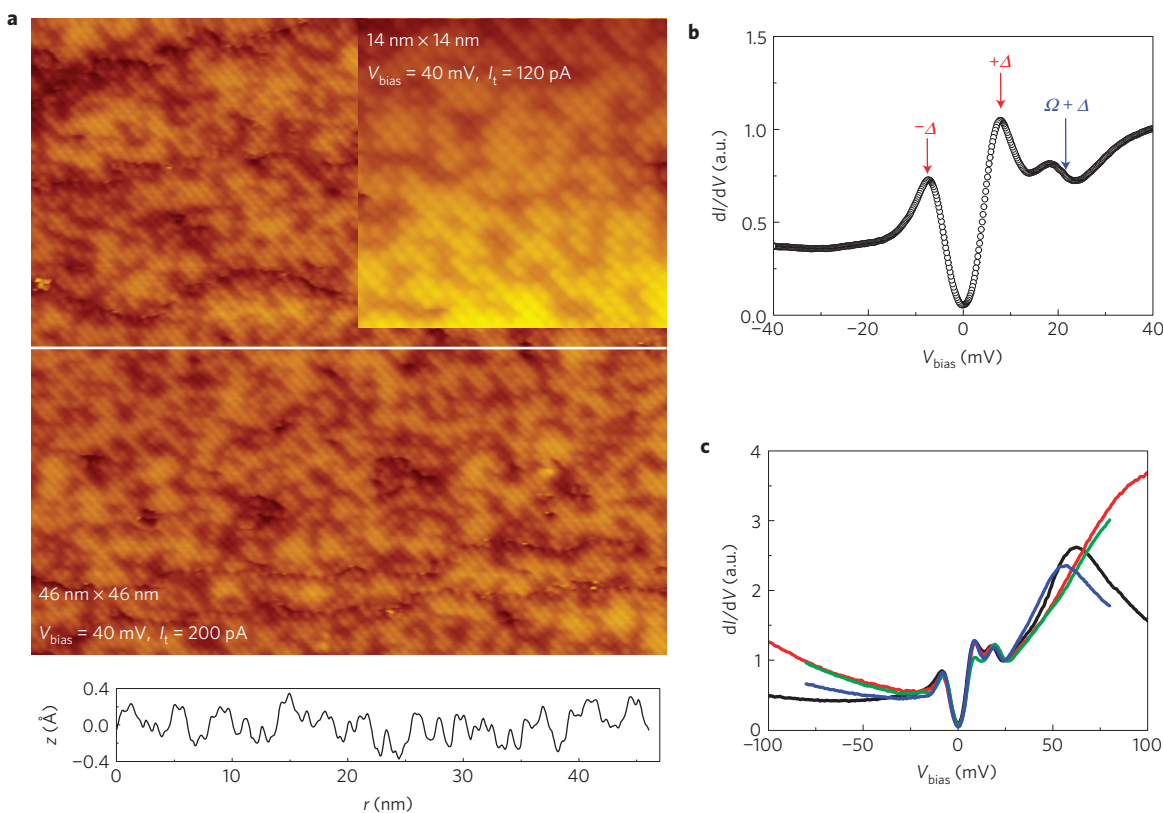


Figure 1 | Topographic STM image and the tunnelling spectra of the $\text{Ba}_{0.6}\text{K}_{0.4}\text{Fe}_2\text{As}_2$ single crystal. a, STM image showing an atomically resolved square lattice with a constant of 5.4 \AA . The inset in **a** shows a closer view. The curve below **a** shows a height distribution measured along the white line marked in **a**. **b**, A typical tunnelling spectrum measured at 1.7 K . The superconducting coherence peaks are marked with arrows labelled Δ and $-\Delta$. The $\Omega + \Delta$ arrow reflects the position of the bosonic mode. A clear asymmetric spectrum is observed, which may be induced by the shallow bands close to the Fermi energy. **c**, Several typical tunnelling spectra measured to a wider energy, exhibiting a hump at about 60 mV or higher energies. The curves with different colours represent the results measured at randomly selected sites.

we find that the ratio is actually very close to the chemical doping ratio $\text{Ba}/\text{K} = 6/4$, indicating that the surface layer is composed of Ba and K atoms. The high quality of the sample is justified by the data in Supplementary Fig. S1. Figure 1b shows a typical tunnelling spectrum measured on the surface. Several interesting features can be seen. The tunnelling spectrum exhibits two clear peaks at an energy level of about $\pm 7.3 \text{ meV}$, which are associated with the superconducting gaps. Another peak appears at an energy of about $21.5 \pm 0.8 \text{ meV}$ (determined at the middle of the right wing of the peak, addressed later). Apparently both the superconducting coherence peak and the peak at about $21.5 \pm 0.8 \text{ meV}$ are more prominent on the right-hand side. We determined the mode energy at the middle of the right wing of the peak because this was adopted in the conventional superconductors to determine the phonon energy, according to the Eliashberg theory^{1–4}. For unconventional superconductors with sign-reversing gaps, the peak (as a consequence of the sign-reversing gap) position depends on the superconducting energy gap as well as the correlation effect^{16–19}. We will come to this point later. The spectrum is quite asymmetric. As shown in Fig. 1c, the DOS is generally low in the negative bias side, and gets much higher at positive bias voltage. On some curves, a peak appears at about 60 mV , and it can even move to higher energies at different sites, but the feature of superconductivity in the low-energy region shows no obvious change. This asymmetric feature can be well explained as a result of the band-edge effect. In fact, in the angle-resolved photoemission spectroscopy data, there are indeed several bands close to the Fermi energy (within 100 meV ; refs 20,21). The peak with a characteristic energy of about 60 mV or higher may be induced by the accumulation of DOS of both

the electron and hole bands. Our simulation shows that indeed this band-edge effect can strongly enhance the DOS as well as the related features in the positive bias side (see later).

To determine whether this mode is closely related to superconductivity, we investigate the temperature and magnetic field dependence of the tunnelling spectra. Figure 2a shows the evolution of the STS spectra with temperatures up to 40 K , which is just above T_c . The black solid lines shown together represent those resulting from performing Fermi–Dirac convolution on the data at 1.7 K (ref. 22). It is clear that at 40 K the mode feature is almost invisible compared with the convoluted data of 1.7 K . Therefore, both the superconducting coherence peak and the mode are suppressed and smeared out with increasing temperature and finally disappear above T_c . To gain a comprehensive understanding of the data, we normalize the dI/dV versus V spectrum measured at different temperatures by the one measured at 40 K (Fig. 2b). Shown here together are theoretical curves (colour lines) calculated using two anisotropic s -wave gaps based on the Dynes model²³. In fact, the calculation with one single anisotropic gap can also fit the data. Both ways yield a dominant gap of $7.3 \pm 0.5 \text{ meV}$, which is close to our previous results of STM measurements on the same kind of samples²⁴. Details of the fitting are given in the Supplementary Information. To illustrate the relationship between superconductivity and the bosonic mode, we determine the area of both the coherence peak and the mode under the tunnelling spectrum. It is known that the tunnelling spectrum would show up as the purple line in Fig. 2c if the electron–boson coupling has no influence; therefore, we determine the weight corresponding to superconductivity by integrating the area under the coherence peak, as marked by the red colour

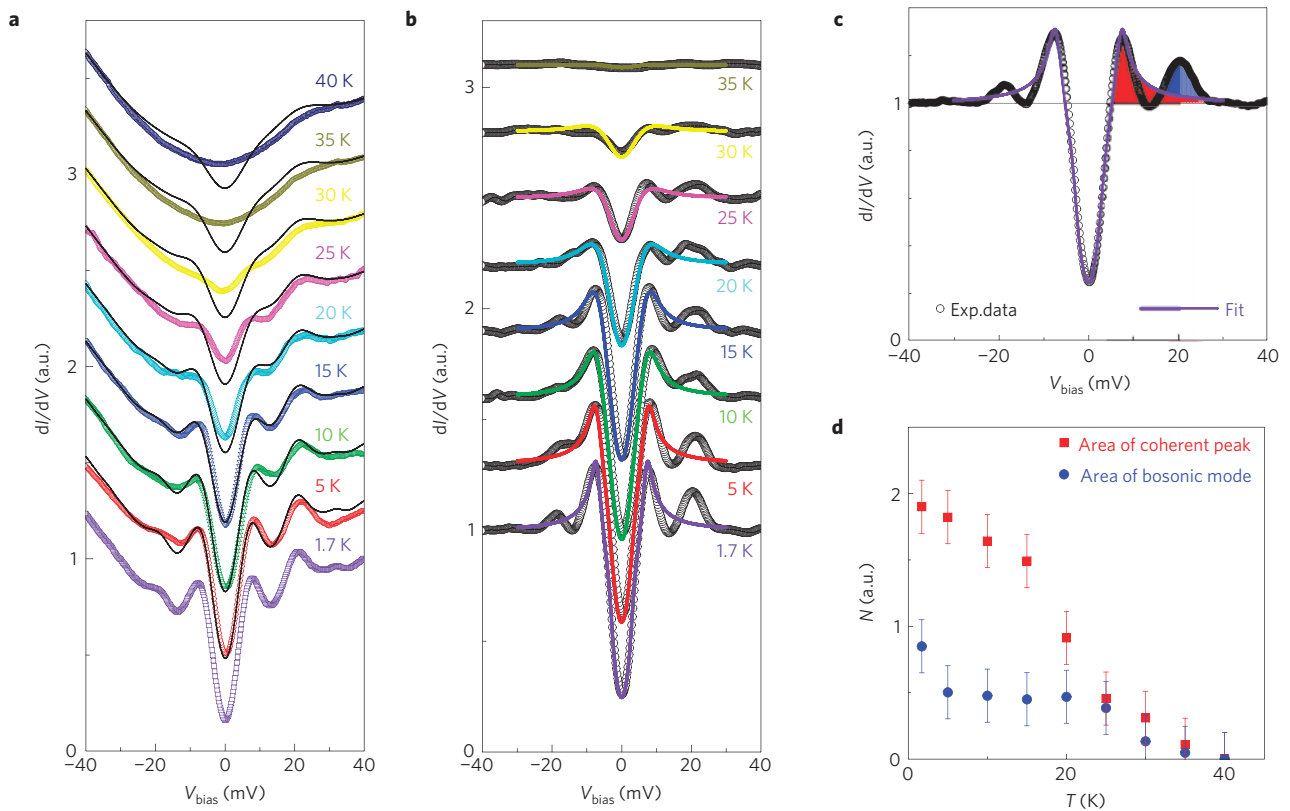


Figure 2 | STS spectra and their temperature dependence for the $\text{Ba}_{0.6}\text{K}_{0.4}\text{Fe}_2\text{As}_2$ single crystal. **a**, The evolution of the STS spectra with temperature increased from 1.7 K to 40 K. Both the coherence peak and mode peak are suppressed and gradually vanish above T_c . The solid lines represent the data at 1.7 K convoluted with the Fermi-Dirac function. **b**, The STS spectra normalized by the one measured in the normal state (at 40 K). The symbols represent the experimental data; the coloured lines are the theoretical fits to the data with the Dynes model with two anisotropic gaps. **c**, The normalized spectrum measured at 1.7 K. The red and the blue areas are those calculated to show the weight of the coherence peak and the bosonic mode. **d**, The temperature dependence of the area of the coherence peak and the mode, as marked by the red and blue areas respectively in **c**. Clearly, they both vanish at about T_c . The error bars in **d** indicate the error from the fitting process using Supplementary Equation S1.

in Fig. 2c. For the bosonic mode, we calculate the area between the mode peak and the calculated curve, as marked by the blue colour in Fig. 2c. The results arising from this calculation about the superconducting coherence peak and the bosonic mode are shown in Fig. 2d. It is evident that both will vanish at T_c , indicating a close relationship between superconductivity and the bosonic mode.

An alternative way to check the relationship between superconductivity and the bosonic mode is to suppress the superconductivity by a high magnetic field and to see how the mode changes inside the vortex core. For this purpose, we applied a magnetic field (11 T) during the measurements. By measuring the two-dimensional spatial distribution of the LDOS at zero energy, we get a vortex pattern with a slightly distorted triangular lattice. Figure 3a shows a high-resolution image of the vortices. It seems that the vortex structure is not as disordered as in $\text{Ba}(\text{Fe}_{1-x}\text{Co}_x)_2\text{As}_2$; this is possibly because the doped atoms go directly to the Fe sites leading to larger disorder in the Co-doped samples²⁵. With the well-measured vortex pattern, we can easily locate and perform careful measurements of the STS curve by crossing one single vortex. By following the trace as marked by the white line in Fig. 3a, we measured the spatially resolved spectra ranging from the outside to the inside of the vortex core. A typical set of data is presented in Fig. 3b. It is clear that, outside the vortex core, the spectrum looks quite similar to that measured at zero magnetic field: a very weak suppression occurs for the coherence peak and the mode feature when the field is applied. However, both peaks are strongly suppressed and even cannot be distinguished from each other when inside the vortex core. Figure 3c shows the spatial evolution of the spectra measured

from the outside to the inside of the vortex cores with a step of 3.6 Å. Both the coherence peak and the mode peak are suppressed simultaneously and finally they are absent; instead a very broad and round hump is formed. To resolve the evolution more clearly, Fig. 3d shows the second derivative curves d^2I/dV^2 versus V . A strong dip appears at about 21.5 ± 0.8 meV, as marked by the dashed line. If we attribute this strong dip to the electron–boson interaction, being analogous to that in the phonon-mediated superconductors, the bosonic mode energy here is about $\Omega = 21.5 - 7.3 = 14.2$ meV. This value is very close to 14–15 meV, the energy of the neutron resonance obtained from the same sample²⁶. It should be noted that neither the kink on the dI/dV versus V curve nor the dip on the d^2I/dV^2 versus V curve at 21.5 ± 0.8 meV change position, seemingly contradicting with a weakened pairing strength when going from the outside to the inside of the vortex core. The apparent gapped feature at the centre of the vortex core is very unusual. A similar phenomenon was observed in the cuprates and explained as being the effect of a competing order^{27,28}. In our present systems, further systematic work is required to solve this issue. Another interesting phenomenon is that in our present study we did not see the in-core Andreev bound state peak, which we observed in previous experiments²⁹. This could be due to several reasons. In the present experiment, the coherence peak arises mainly from the larger gap (7–8 meV), whereas the previous STS curve that exhibits the in-core Andreev bound states mainly comes from the small gap (3–4 meV). According to the extended theory of the S_{\pm} model, the DOS and the gap value of each Fermi surface may have the relation $N_s/N_L = (\Delta_L/\Delta_s)^2$; therefore, the DOS (N_s) on the Fermi surface

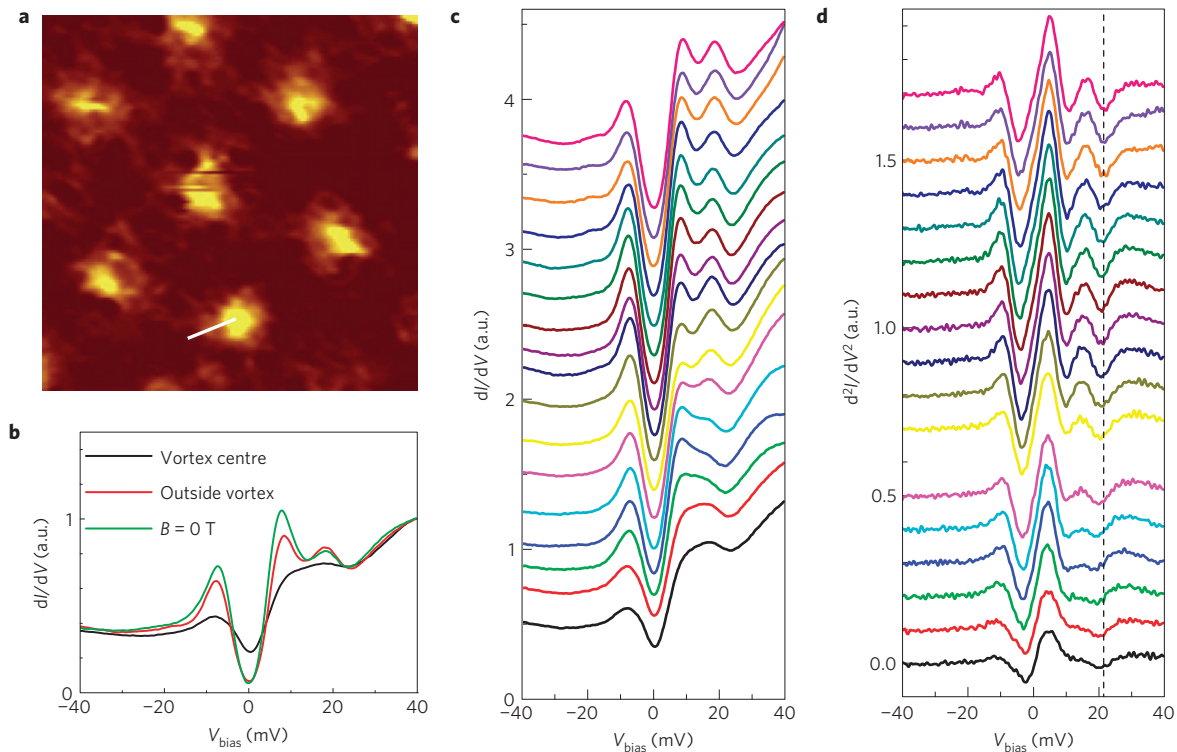


Figure 3 | Spatial mapping of the LDOS and STS spectra across a vortex core on the $\text{Ba}_{0.6}\text{K}_{0.4}\text{Fe}_2\text{As}_2$ single crystal. **a**, A high-resolution topographic image ($39\text{ nm} \times 39\text{ nm}$) of the vortex lattice measured by the LDOS at zero bias. The white line indicates the trace on which the tunnelling spectra shown in **c** were measured. **b**, The tunnelling spectra measured at zero magnetic field (green line), outside the vortex core (red line) and at the centre of the vortex core (dark line) when a 11 T magnetic field is applied. **c**, The spatially resolved tunnelling spectrum dI/dV versus V measured from outside (upper curve) to the centre of the vortex core (bottom) with a step of 3.6 \AA . No in-core Andreev bound state peaks are observed. Both the coherence peak and the mode peak are suppressed and gradually disappear inside the vortex core, showing the close relationship between the superconducting coherence peak and the peak of the bosonic mode. **d**, The second derivative curve d^2I/dV^2 versus V . The bosonic mode appears here at about 21.5 mV as a sharp dip. The dip feature is gradually smeared up inside the vortex core.

of the small gap is much larger than that of the larger gap (N_L); thus, the in-gap Andreev bound states are mainly arising from the DOS of the small gap³⁰. The distinction could be due to the different surface states in these two cases. We must emphasize that the bulk qualities of the two samples are exactly the same; both are very good.

Although we have shown that there is a strong mode feature outside the superconducting gap of $\text{Ba}_{0.6}\text{K}_{0.4}\text{Fe}_2\text{As}_2$, and the mode has a similar energy to the neutron resonance energy, it can still be argued that it could be induced by the interaction between the quasiparticles and the Einstein phonon mode, which probably has an energy, coincidentally, of around 14 meV . To show that this is not the case, we select a totally different system with a different T_c , that is, $\text{Na}(\text{Fe}_{0.975}\text{Co}_{0.025})\text{As}$ ($T_c = 21\text{ K}$). This system is perfect for the STM measurement because we can get a nonpolar surface with well-ordered Na atoms^{22,31,32}. Figure 4a shows the topography of the cleaved surface of this 111 sample with a tunnelling current of $I_t = 200\text{ pA}$ and a voltage of $V = 40\text{ meV}$. Beside the atomic lattice, a block with a rectangular morphology can be seen. This was argued to correspond to one single Co impurity and is discussed elsewhere³². Figure 4c shows the spatial evolution of the tunnelling spectrum along the line marked with blue dots every half lattice constant in Fig. 4a. The STS spectra exhibit a flat zero bottom, indicating a full superconducting gap. Moreover, the superconducting coherence peaks are very clear and strong here, yielding a gap value of about 5.5 meV . This gap value is quite close to that observed by angle-resolved photoemission spectroscopy, which indicates an identical gap on both the hole and electron pockets³³. In addition, just outside the superconducting coherence peak, a small hump appears at an energy of about $13.3 \pm 0.8\text{ meV}$ on both sides.

To show this more clearly, the second derivative curves d^2I/dV^2 are shown in Fig. 4d. A clear dip occurs at an energy of about $13.3 \pm 0.8\text{ meV}$. If we follow the method used for $\text{Ba}_{0.6}\text{K}_{0.4}\text{Fe}_2\text{As}_2$ to determine the mode energy for $\text{Na}(\text{Fe}_{0.975}\text{Co}_{0.025})\text{As}$, that would give $\Omega = 13.3 - 5.5 \approx 7.8\text{ meV}$. Figure 4b shows the difference in the imaginary part of the spin susceptibility measured at 5 and 25 K. A resonance peak appears at around 7 meV at $Q = (1/2, 1/2, 2)$. This resonance energy once again is very close to the mode energy determined from the tunnelling measurement. Figure 5a presents the temperature dependence of the tunnelling spectrum, showing again both the superconducting coherence peak and the mode at 1.7 K . With increasing temperature, both features are weakened simultaneously and vanish above T_c . In all of the STS curves, we see a clear asymmetry. This asymmetry extends even to a temperature well above T_c . This asymmetry, as seen in $\text{Ba}_{0.6}\text{K}_{0.4}\text{Fe}_2\text{As}_2$, is argued to be the result of the band-edge effect. Interestingly, as shown in Fig. 2a, when there is a weak anomaly feature on the positive bias side in the normal state, the superconducting coherence peak and the mode feature are enhanced also on the same side. By taking the data at 25 K ($> T_c = 21\text{ K}$) as the background and dividing the STS data measured at all other temperatures by this background, we get STS spectra with a more symmetric shape (Fig. 5b). After doing this, the mode feature becomes very clear. By applying a magnetic field of 11 T at 1.7 K , we measured the spatial distribution of the LDOS at zero energy. The data are presented in Fig. 5c, in which a slightly distorted triangle vortex lattice can again be seen in this sample. Figure 5d shows the spatial evolution of the STS spectra measured along the arrowed white line indicated in Fig. 5c. A very similar feature as observed in $\text{Ba}_{0.6}\text{K}_{0.4}\text{Fe}_2\text{As}_2$ can be seen. It

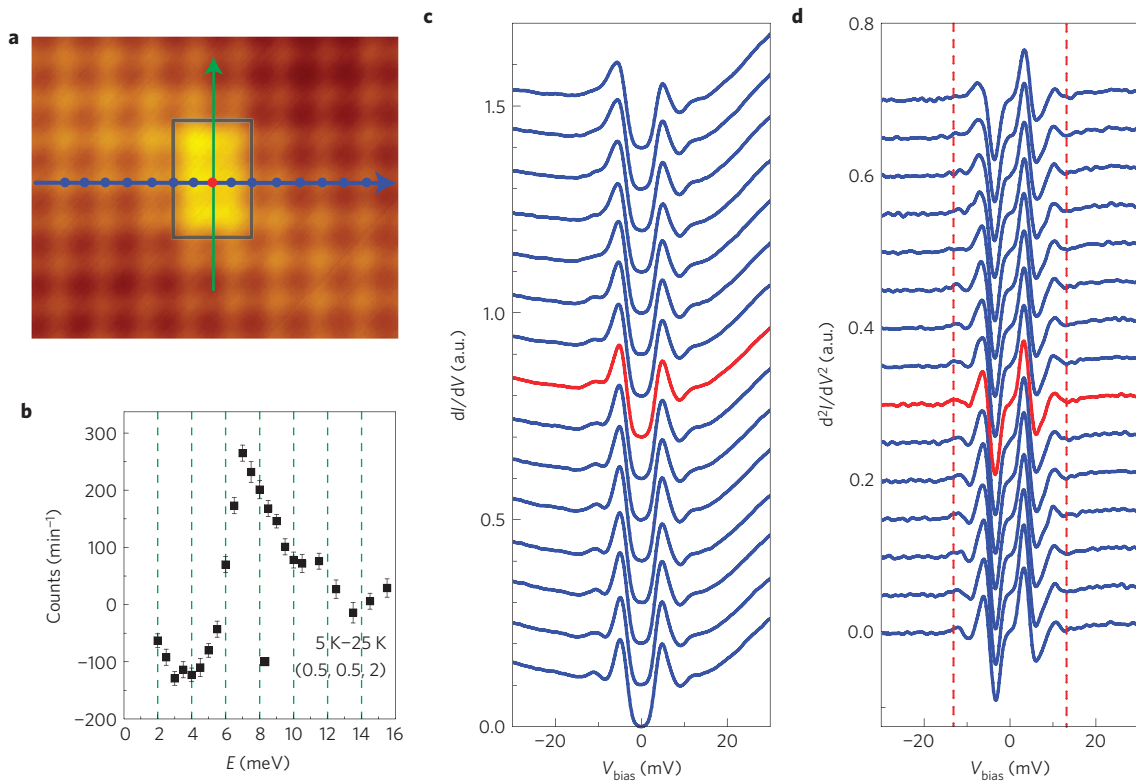


Figure 4 | Spatially resolved STS spectra on $\text{Na}(\text{Fe}_{0.975}\text{Co}_{0.025})\text{As}$ single crystal. **a**, Spatially resolved atomic lattice with a constant of 3.80 \AA measured with a tunnelling current of $I_t = 200 \text{ pA}$ and a voltage of $V = 40 \text{ meV}$. A rectangular shape with 2×3 atoms is observed, which is well associated with a single Co impurity in the middle and will be presented elsewhere. **b**, The difference in the imaginary part of the spin susceptibility measured at 5 and 25 K. A resonance peak appears around 7 meV at $Q = (1/2, 1/2, 2)$. **c**, The tunnelling spectra measured at zero magnetic field at the positions marked by the blue dots in **a**. The red line represents the one detected at the centre of the 2×3 rectangular block, assumed to be the site of the Co impurity. **d**, The second derivative curve d^2I/dV^2 versus V . The bosonic mode is marked by the dashed line, where a dip appears at about 13.5 mV. The error bars in **b** indicate statistical errors of one standard deviation.

is clear that both the superconducting coherence peak and the mode feature observed outside the gap are suppressed simultaneously. It is interesting that the STS spectrum measured at the vortex core looks quite similar to that measured above T_c . This asymmetric background both at the vortex core centre and above T_c is also observed in LiFeAs (refs 22,31), and is naturally explained as being due to the shallow band-edge effect.

The coincidence of the bosonic mode energy and the neutron resonance energy in two completely different systems is quite intriguing and indicates that the mode feature is unlikely induced by phonons. Given the pronounced differences in the crystal structures between $\text{Ba}_{0.6}\text{K}_{0.4}\text{Fe}_2\text{As}_2$ and $\text{Na}(\text{Fe}_{0.975}\text{Co}_{0.025})\text{As}$, it is difficult to imagine that two phonons would occur at exactly the energy of the resonance for the two systems. Therefore, our results suggest that the electrons are strongly coupled to the spin excitations. By taking account of the ratio between Ω and T_c , there is a universal ratio in the two different samples: $\Omega/k_B T_c = 14.2 \times 11.6/38 = 4.33 \pm 0.25$ in $\text{Ba}_{0.6}\text{K}_{0.4}\text{Fe}_2\text{As}_2$ and $7.8 \times 11.6/21 = 4.31 \pm 0.44$ in $\text{Na}(\text{Fe}_{0.975}\text{Co}_{0.025})\text{As}$ (taking $\pm 0.8 \text{ meV}$ as the error bar for Ω). In the optimally doped $\text{Ba}(\text{Fe}_{1-x}\text{Co}_x)_2\text{As}_2$, because no STM data have been reported so far for the bosonic mode, we take the value of the neutron resonance energy, which is about 9.5 meV (ref. 34), and using $T_c = 25 \text{ K}$, we get $E_r/k_B T_c = 4.28$. Meanwhile it is concluded that there is a universal ratio³⁵ between the resonance energy E_r and T_c , which is about 4.6 in many types of iron pnictide superconductor. Figure 6 shows the resonance energy derived from the neutron scattering experiments as open symbols^{13,26,34–43} for different systems, versus the superconducting transition temperatures. The

mode energy determined from our tunnelling measurements is also plotted. Remarkably, our data points fall quite well onto the so-called universal plot.

The close relationship between the electron tunnelling mode and neutron spin resonance in two different systems strongly suggests that the pairing should have a magnetic origin. In this context, there are two scenarios to explain the neutron resonance and the mode feature in tunnelling measurements: it is the consequence of the sign-reversal of the gap; it is this mode that mediates the pairing, namely it acts as the pairing glue. Now we discuss these two possibilities. A general argument against the idea of pairing glue for the neutron spin resonance stems from two concerns: the absolute weight of the neutron resonance mode is too weak to account for the superconducting condensation in most unconventional superconductors¹⁷, although in optimally doped $\text{YBa}_2\text{Cu}_3\text{O}_{7-\delta}$ the mode seems to have sufficient weight to account for the superconducting condensation energy⁴⁴; and more seriously, the mode vanishes above T_c in optimally doped superconductors, which is not like the phonon that persists all the way crossing T_c . According to the Eliashberg theory on superconductors with a sign-reversing gap, a resonance mode due to the particle hole excitation will be formed within 2Δ (refs 16–19). From a general point of view, the mode energy may be written as $\Omega = 2\Delta[1 - f(U/t)]$ with an unknown function $f(U/t)$ being less than 1 and depending on the ratio between the repulsive energy U and the kinetic energy t . Assuming that $\Delta \approx 2 \sim 2.5 k_B T_c$ in the case of strong coupling, we indeed have $\Omega/k_B T_c \approx 4\text{--}5$ if the correlation is mild ($f(U/t) \ll 1$). Theoretically, a precise expression for $f(U/t)$ is still lacking. In addition, by following this argument, as far as we know, there is

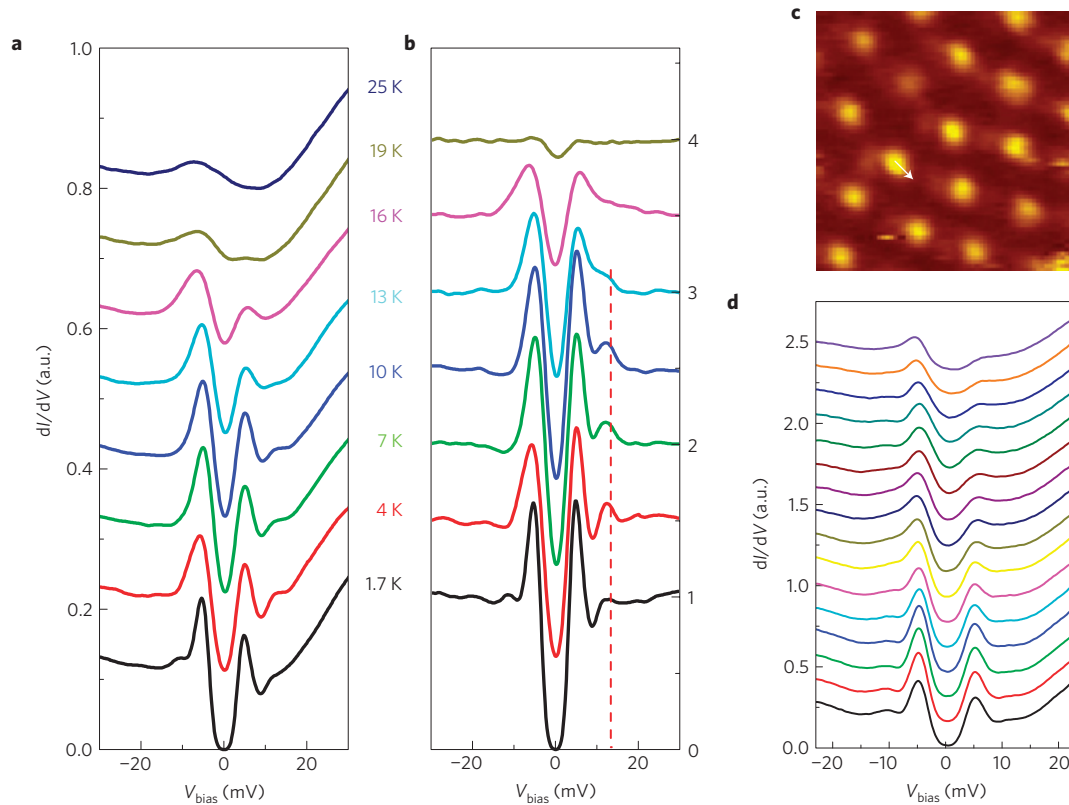


Figure 5 | Temperature dependence of the tunnelling spectra for the Na(Fe_{0.975}Co_{0.025})As single crystal. **a**, The evolution of the STS spectra with temperature increased from 1.7 K to 25 K. A small hump appears above the superconducting coherence peak. All spectra are asymmetric with an enhancement on the left-hand side, which is attributed to the band-edge effect. **b**, The STS spectra normalized by the one measured in the normal state (at 25 K). **c**, A high-resolution topographic image (39 nm × 39 nm) of the vortex lattice measured by the LDOS at a magnetic field of 11 T, showing a slightly distorted vortex lattice structure. The white arrowed line indicates the trace on which the spectra shown in **d** were measured. **d**, Spatially resolved tunnelling spectra dI/dV versus V measured from the outside (bottom curve) to the centre of the vortex core (upper) with a step of 3.6 \AA .

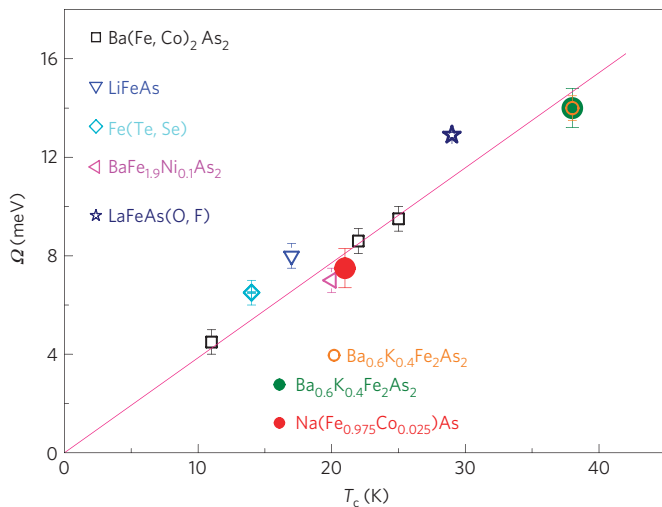


Figure 6 | A universal relation between the mode energy and the superconducting transition temperature T_c . The open points with error bars represent the neutron resonance energies versus T_c for many different samples; the filled dark green and red circles show the mode energy Ω versus T_c of our tunnelling experiments on the Ba_{0.6}K_{0.4}Fe₂As₂ and Na(Fe_{0.975}Co_{0.025})As single crystals, respectively. The red line shows a universal relation: $(E_r, \Omega)/k_B T_c = 4.4$. The error bars for the data in this work indicate the standard deviation of the Gaussian distribution fitting of Ω ; those for the open symbols are taken from the literature.

no explicit way to prove that the mode feature should locate at the dip position of the second derivative curve d^2I/dV^2 versus V , as observed in our data and the phonon-mediated superconductors¹⁻⁴. Therefore, our results will stimulate further theoretical efforts to get a quantitative understanding.

The other scenario concerns the bosonic mode as the pairing glue. To get a basic assessment of this model, and especially for understanding the asymmetry of the mode features with respect to the Fermi level, we performed self-consistent microscopic calculations using the four-band (two electron and two hole bands) Eliashberg formalism. This type of theory was applied for the d -wave pairing in cuprates with the assumption that the electrons are coupled to the resonance spin fluctuation mode revealed by inelastic neutron scattering^{45,46}. Along a similar line, we assume that the observed $(\pi, 0)$ neutron resonance mode (for example, 14 meV in Ba_{0.6}K_{0.4}Fe₂As₂) mediates pairing in the present system. The detailed simulation process is presented in the Supplementary Information and the results are given in Supplementary Figs S3 and S4. It is found that the theoretical simulation can capture the basic features of the tunnelling spectra by properly choosing the fitting parameters. In particular, in this simulation, the mode feature is situated at the dip position of the second derivative curve d^2I/dV^2 versus V . However, the strength of the mode feature at the energy $\Delta + \Omega$ simulated by the Eliashberg theory is much weaker than the experimental one shown in Fig. 2b. The fact that the tunnelling mode feature disappears above T_c and inside the vortex core, and its energy is at $\Delta + \Omega$, suggest that the peak should be strongly related to superconductivity. The universal ratio of $\Omega/k_B T_c \approx 4.3$ in two different systems with distinct transition temperatures and

the coincidence with the neutron resonance support the picture of pairing through spin fluctuations, although the bosonic mode itself may be a consequence of the sign-reversing superconducting gap.

Received 11 April 2012; accepted 11 October 2012; published online 18 November 2012

References

- Rowell, J. M., Anderson, P. W. & Thompson, D. E. Image of the phonon spectrum in the tunneling characteristics between superconductors. *Phys. Rev. Lett.* **10**, 334–336 (1963).
- Schrieffer, J. R., Scalapino, D. J. & Wilkins, J. W. Effective tunneling density of states. *Phys. Rev. Lett.* **10**, 336–339 (1963).
- Swihart, J. C., Scalapino, D. J. & Wada, Y. Solution of the gap equations for Pb, Hg, and Al. *Phys. Rev. Lett.* **14**, 106–108 (1965).
- McMillan, W. L. & Rowell, J. M. Lead phonon spectrum calculated from superconducting density of states. *Phys. Rev. Lett.* **14**, 108–111 (1965).
- Lee, J. *et al.* Interplay of electron-lattice interactions and superconductivity in $\text{Bi}_2\text{Sr}_2\text{CaCu}_2\text{O}_{8+\delta}$. *Nature* **442**, 546–550 (2006).
- Hwang, J., Timusk, T. & Carbotte, J. P. Scanning-tunneling spectra of cuprates. *Nature* **446**, E3–E4 (2007).
- Cuk, T. *et al.* A review of electron–phonon coupling seen in the high- T_c superconductors by angle-resolved photoemission studies (ARPES). *Phys. Stat. Sol.* **242**, 11–29 (2005).
- Niستمسكي, F. C. *et al.* A distinct bosonic mode in an electron-doped high-transition-temperature superconductors. *Nature* **450**, 1058–1061 (2007).
- Wilson, S. D. *et al.* Resonance in the electron-doped high-transition-temperature superconductor $\text{Pr}_{0.88}\text{LaCe}_{0.12}\text{CuO}_{4-\delta}$. *Nature* **442**, 59–62 (2006).
- Jin, K., Butch, N. P., Kirshenbaum, K. & Greene, R. L. Link between spin fluctuations and electron pairing in copper oxide superconductors. *Nature* **476**, 73–75 (2011).
- Mazin, I. I., Singh, D. J., Johannes, M. D. & Du, M. H. Unconventional sign-reversing superconductivity in $\text{LaFeAsO}_{1-x}\text{F}_x$. *Phys. Rev. Lett.* **101**, 057003 (2008).
- Kuroki, K. *et al.* Unconventional pairing originating from the disconnected Fermi surfaces of superconducting $\text{LaFeAsO}_{1-x}\text{F}_x$. *Phys. Rev. Lett.* **101**, 087004 (2008).
- Christianson, A. D. *et al.* Unconventional superconductivity in $\text{Ba}_{0.6}\text{K}_{0.4}\text{Fe}_2\text{As}_2$ from inelastic neutron scattering. *Nature* **456**, 930–932 (2008).
- Hanaguri, T., Niitaka, S., Kuroki, K. & Takagi, K. Unconventional s -wave superconductivity in $\text{Fe}(\text{Se},\text{Te})$. *Science* **328**, 474–476 (2010).
- Shan, L. *et al.* Evidence of a spin resonance mode in the iron-based superconductor $\text{Ba}_{0.6}\text{K}_{0.4}\text{Fe}_2\text{As}_2$ from scanning tunneling spectroscopy. *Phys. Rev. Lett.* **108**, 227002 (2012).
- Abanov, Ar., Chubukov, A. V., Eschrig, M., Norman, M. R. & Schmalian, J. The neutron resonance in the cuprates and its effect on fermionic excitations (What the resonance peak can do). *Phys. Rev. Lett.* **89**, 177002 (2002).
- Kee, H. Y., Kivelson, S. A. & Aeppli, G. Spin-1 neutron resonance peak cannot account for electronic anomalies in the cuprate superconductors. *Phys. Rev. Lett.* **88**, 257002 (2002).
- Eremin, I., Morr, D. K., Chubukov, A. V., Bennemann, K. H. & Norman, M. R. Novel neutron resonance mode in $d_{x^2-y^2}$ -wave superconductors. *Phys. Rev. Lett.* **94**, 147001 (2005).
- Balatsky, A. V. & Zhu, J. X. Local strong-coupling pairing in d -wave superconductors with inhomogeneous bosonic modes. *Phys. Rev. B* **74**, 094517 (2006).
- Ding, H. *et al.* Electronic structure of optimally doped pnictide $\text{Ba}_{0.6}\text{K}_{0.4}\text{Fe}_2\text{As}_2$: A comprehensive ARPES investigation. *J. Phys. Condens. Matter* **23**, 135701 (2011).
- Evtushinsky, D. V. *et al.* Fusion of bogoliubons in $\text{Ba}_{0.6}\text{K}_{0.4}\text{Fe}_2\text{As}_2$ and similarity of energy scales in high temperature superconductors. Preprint at <http://arxiv.org/abs/1106.4584> (2011).
- Hanaguri, T. *et al.* Scanning tunneling microscopy/spectroscopy of vortices in LiFeAs . *Phys. Rev. B* **85**, 214505 (2012).
- Dynes, R. C., Garno, J. P., Hertel, G. B. & Orlando, T. P. Tunneling study of superconductivity near the metal-insulator transition. *Phys. Rev. Lett.* **53**, 2437–2440 (1984).
- Shan, L. *et al.* Evidence of multiple nodeless energy gaps in superconducting $\text{Ba}_{0.6}\text{K}_{0.4}\text{Fe}_2\text{As}_2$ single crystals from scanning tunneling spectroscopy. *Phys. Rev. B* **83**, 060510 (2011).
- Yin, Y. *et al.* Scanning tunneling spectroscopy and vortex imaging in the iron pnictide superconductor $\text{BaFe}_{1.8}\text{Co}_{0.2}\text{As}_2$. *Phys. Rev. Lett.* **102**, 097002 (2009).
- Zhang, C. L. *et al.* Neutron scattering studies of spin excitations in hole-doped $\text{Ba}_{0.67}\text{K}_{0.33}\text{Fe}_2\text{As}_2$ superconductor. *Sci. Rep.* **1**, 115 (2011).
- Hoffman, J. E. *et al.* Imaging quasiparticle interference in $\text{Bi}_2\text{Sr}_2\text{CaCu}_2\text{O}_{8+\delta}$. *Science* **297**, 1148–1151 (2002).
- Pan, S. H. *et al.* STM studies of the electronic structure of vortex cores in $\text{Bi}_2\text{Sr}_2\text{CaCu}_2\text{O}_{8+\delta}$. *Phys. Rev. Lett.* **85**, 1536–1539 (2000).
- Shan, L. *et al.* Observation of ordered vortices with Andreev bound states in $\text{Ba}_{0.6}\text{K}_{0.4}\text{Fe}_2\text{As}_2$. *Nature Phys.* **4**, 325–331 (2011).
- Mazin, I. I. & Schmalian, J. Pairing symmetry and pairing state in ferropnictides: Theoretical overview. *Physica C* **469**, 614–627 (2009).
- Hänke, T. *et al.* Probing unconventional superconductivity in LiFeAs by quasiparticle interference. *Phys. Rev. Lett.* **108**, 127001 (2011).
- Yang, H. *et al.* Unexpected weak spatial variation of local density of states induced by individual Co impurity atoms in $\text{Na}(\text{Fe}_{0.95}\text{Co}_{0.05})\text{As}$ as revealed by scanning tunneling spectroscopy. Preprint at <http://arxiv.org/abs/1203.3123> (2012).
- Liu, Z.-H. *et al.* Unconventional superconducting gap in $\text{NaFe}_{0.95}\text{Co}_{0.05}\text{As}$ observed by angle-resolved photoemission spectroscopy. *Phys. Rev. B* **84**, 064519 (2011).
- Inosov, D. S. *et al.* Normal-state spin dynamics and temperature-dependent spin resonance energy in optimally doped $\text{BaFe}_{1.85}\text{Co}_{0.15}\text{As}_2$. *Nature Phys.* **6**, 178–181 (2010).
- Inosov, D. S. *et al.* Crossover from weak to strong pairing in unconventional superconductors. *Phys. Rev. B* **83**, 214520 (2011).
- Christianson, A. D. *et al.* Static and dynamic magnetism in underdoped superconductor $\text{BaFe}_{1.92}\text{Co}_{0.08}\text{As}_2$. *Phys. Rev. Lett.* **103**, 087002 (2009).
- Taylor, A. E. *et al.* Antiferromagnetic spin fluctuations in LiFeAs observed by neutron scattering. *Phys. Rev. B* **83**, 220514 (2011).
- Mook, H. A. *et al.* Unusual relationship between magnetism and superconductivity in $\text{FeTe}_{0.5}\text{Se}_{0.5}$. *Phys. Rev. Lett.* **104**, 187002 (2010).
- Qiu, Y. M. *et al.* Spin gap and resonance at the nesting wave vector in superconducting $\text{FeSe}_{0.4}\text{Te}_{0.6}$. *Phys. Rev. Lett.* **103**, 067008 (2009).
- Babkevich, P. *et al.* Spin anisotropy of the resonance peak in superconducting $\text{FeSe}_{0.5}\text{Te}_{0.5}$. *Phys. Rev. B* **83**, 180506 (2011).
- Chi, S. X. *et al.* Inelastic neutron-scattering measurements of a three-dimensional spin resonance in the FeAs-based $\text{BaFe}_{1.9}\text{Ni}_{0.1}\text{As}_2$ superconductor. *Phys. Rev. Lett.* **102**, 107006 (2009).
- Lumsden, M. D. *et al.* Two-dimensional resonant magnetic excitation in $\text{BaFe}_{1.84}\text{Co}_{0.16}\text{As}_2$. *Phys. Rev. Lett.* **102**, 107005 (2009).
- Wakimoto, S. *et al.* Degradation of superconductivity and spin fluctuations by electron overdoping in $\text{LaFeAsO}_{1-x}\text{F}_x$. *J. Phys. Soc. Jpn* **79**, 074715 (2010).
- Woo, H., Dai, P. C., Hayden, S. M., Mook, H. A. & Dahm, T. E. Magnetic energy change available to superconducting condensation in optimally doped $\text{YBa}_2\text{Cu}_3\text{O}_{6.95}$. *Nature Phys.* **2**, 600–604 (2006).
- Abanov, Ar., Chubukov, A. V. & Schmalian, J. Fingerprints of spin mediated pairing in cuprates. *J. Electron Spectros. Relat. Phenom.* **117–118**, 129–151 (2001).
- Castellan, J. P. *et al.* Effect of Fermi surface nesting on resonant spin excitations in $\text{Ba}_{1-x}\text{K}_x\text{Fe}_2\text{As}_2$. *Phys. Rev. Lett.* **107**, 177003 (2011).

Acknowledgements

We acknowledge useful discussions with A. V. Chubukov, S. Kivelson, M. Norman, I. I. Mazin, I. Eremin and A. Balatsky. We especially thank A. A. Golubov, J. Schmalian and I. I. Mazin for their preliminary calculations in helping us to understand the data based on the Eliashberg theory. This work was supported by the NSF of China, the Ministry of Science and Technology of China (973 projects: 2011CBA00100, 2012CB821403, 2012CB21400, 2010CB923002, 2011CB922101) and PAPD. The single-crystal growth effort at UTK is supported by the US DOE BES No. DE-FG02-05ER46202.

Author contributions

The low-temperature STS measurements were performed by Z.W., H.Y. and D.F., with help from H.-H.W. and L.S. The samples were prepared by B.S. and C.Z. The simulation based on the Eliashberg theory was performed by Q.-H.W. H.-H.W. coordinated the whole work and wrote the manuscript, which was supplemented by Q.-H.W., Z.W. and H.Y., and revised by P.D. All authors have discussed the results and the interpretation.

Additional information

Supplementary information is available in the online version of the paper. Reprints and permissions information is available online at www.nature.com/reprints. Correspondence and requests for materials should be addressed to H.-H.W.

Competing financial interests

The authors declare no competing financial interests.